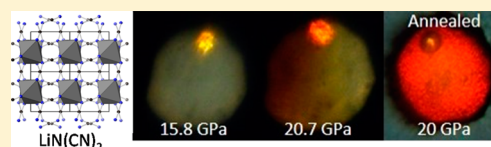


HPSTAR
257-2016Pressure-Induced Polymerization of $\text{LiN}(\text{CN})_2$ Derek W. Keefer,^{*,†} Huiyang Gou,^{‡,||} Andrew P. Purdy,[§] Albert Epshteyn,[§] Duck Young Kim,^{‡,||} John V. Badding,^{†,‡,Δ,◇} and Timothy A. Strobel^{*,‡}[†]Department of Chemistry, [‡]Department of Physics, ^ΔDepartment of Materials Science and Engineering, and [◇]Materials Research Institute, The Pennsylvania State University, University Park, Pennsylvania 16802, United States[‡]Geophysical Laboratory, Carnegie Institution of Washington, 5251 Broad Branch Road NW, Washington, DC, 20015, United States[§]Chemistry Division, Naval Research Laboratory, 4555 Overlook Avenue, SW, Washington, DC, 20375, United States^{||}Center for High Pressure Science and Technology Advanced Research, 1690 Cailun Road, Bldg #6, Pudong, Shanghai 201203, China.

ABSTRACT: The high-pressure behavior of lithium dicyanamide ($\text{LiN}(\text{CN})_2$) was studied with in situ Raman and infrared (IR) spectroscopies, and synchrotron angle-dispersive powder X-ray diffraction (PXRD) in a diamond anvil cell (DAC) to 22 GPa. The fundamental vibrational modes associated with molecular units were assigned using a combination of experimental data and density functional perturbation theory. Some low-frequency modes were observed for the first time. On the basis of spectroscopic and diffraction data, we suggest a polymorphic phase transformation at ~ 8 GPa, wherein dicyanamide ions remain as discrete molecular species. Above ca. 18 GPa, dicyanamide units polymerize, forming a largely disordered network, and the extent of polymerization may be increased by annealing at elevated temperature. The polymerized product consists of tricyanomelaminite-like groups containing sp^2 -hybridized carbon–nitrogen bonds and exhibits a visible absorption edge near 540 nm. The product is recoverable to ambient conditions but is not stable in air/moisture.



I. INTRODUCTION

Carbon's ability to possess variable orbital hybridization schemes gives it the properties of diamond, the hardest material known, and of graphite, one of the softest.¹ Likewise, CN compounds can potentially exist with sp^3 hybridization and as graphitic-type materials, both analogous to diamond and graphite, respectively.^{2,3} To date, only the formation of sp^2 carbon–nitrogen networks is well-established, and significant challenges remain in accessing novel, three-dimensional CN-based extended solids with computationally predicted energetic feasibility.^{2–8} In addition to three-dimensional systems, fully sp^2 CN-rich materials are also of great interest from the standpoint of fundamental chemical transformations, as well as practical applications in catalysis and energy conversion.^{9–12} One strategy to synthesize novel CN-rich solids is to begin with highly unsaturated carbon–nitrogen building blocks, lacking hydrogen or amine functionalities, that will react into extended networks after modest pressures are applied with full atom economy (sans release of byproducts). By starting from metastable molecules (building blocks) in a high-energy state, subsequent rearrangement into a lower-energy extended network is thermodynamically favored and may be facilitated by topochemical considerations.^{13–16}

Dicyanamides represent one class of possible building blocks with a high concentration of CN units and have been produced with a variety of alkali metals (Li, Na, K, Rb, Cs), alkaline earth metals (Mg, Ca, Sr, Ba), and rare earth metals (La, Ce, Pr, Nd, Sm, Eu, Gd).^{17–22} Rare earth metal CN networks have been used to make frameworks that are particularly interesting for

studying molecular magnets and organic superconductors.²³ Dicyanamides have seen commercial application as airbag components.²⁴ Studies on metal (M)–dicyanamides have used heat as a perturbative variable, causing them to react and polymerize into extended structures.^{17,20}

It has been well established that dicyanamide anions can go through a trimerization process.^{25–27} This process involves three cyanide groups from different dicyanamide ions coming together to form a tricyanomelaminite ring. Jurgens et al. reported that the trimerization process proceeds at ambient pressure and temperatures >613 K in the crystalline state with no observed intermediates or melting.²⁵ Tricyanomelaminite is of interest because it contains a C_3N_3 triazine ring structure, which has been studied for understanding the formation of graphitic carbon nitrides.^{25,28–30}

The binary CN system (as well as other multicomponent analogues) has the potential for structural flexibility similar to that of pure carbon, but precursor-based synthetic strategies have not been thoroughly explored under pressure. The unsaturated nitrile group has the potential to form new bonds under pressure through cycloaddition-type reactions and could possibly result in the formation of extended network solids.³¹ A detailed analysis of the vibrational and structural evolution under pressure is of great importance in understanding the transformation from the highly unsaturated

Received: July 6, 2016

Revised: October 27, 2016

Published: October 28, 2016

building-block to an interconnected network, providing fundamental information regarding the evolution of CN bonding and reaction mechanisms.^{31,32}

In this study, we present in situ, high-pressure spectroscopic and structural results for $\text{LiN}(\text{CN})_2$ compressed to 22 GPa. Raman and IR spectroscopies were used to probe the evolution of CN bonding, whereas synchrotron PXRD was used to obtain structural information. With these methodologies, a partially amorphous network comprising tricyanomelaminite-like groups was successfully synthesized through the polymerization of lithium dicyanamide.

II. METHODS

IIA. Synthesis. Anhydrous $\text{LiN}(\text{CN})_2$ was prepared in a manner very similar to that in a previous report.²⁷ The as-purchased $\text{NaN}(\text{CN})_2$ (Alfa-Aesar) was recrystallized from water and dried under vacuum. Anhydrous LiCl (4.53 g, 107 mmol) was stirred under argon with a slight excess of $\text{NaN}(\text{CN})_2$ (10.00 g, 112 mmol) in dry THF (33 g) at 100 °C in a closed H-tube for 3 days and filtered. After solvent removal under vacuum, the crude $\text{LiN}(\text{CN})_2$ was dissolved in boiling dry MeCN and the solution was allowed to cool. The liquid was decanted and the crystals were pumped dry with mild heating to afford anhydrous $\text{LiN}(\text{CN})_2$ (7.17 g, 87%), which was handled only in a drybox.

IIB. DFPT Calculations. Raman intensity calculations were performed using density functional perturbation theory³³ implemented in the Quantum Espresso software.³⁴ For exchange and correlation functional, Perdew–Burke–Ernzerhof parametrization³⁵ of the generalized gradient approximation was used. For electronic structure calculations and DFPT calculations, a uniform $6 \times 6 \times 4$ grid of k point mesh used with a cutoff energy of 1100 eV for the plane wave expansion of wave functions.

IIC. Sample Preparation. Samples of $\text{LiN}(\text{CN})_2$ were ground in an agate mortar to a fine powder ($\sim 5 \mu\text{m}$) under an inert argon atmosphere ($\text{O}_2 < 0.5 \text{ ppm}$, $\text{H}_2\text{O} < 0.5 \text{ ppm}$). This powder and a ruby sphere were loaded into DACs with culet sizes ranging between 300 and 500 μm . The DAC was prepared by preindenting a rhenium gasket to a thickness between 50 and 70 μm . The sample chamber was prepared by drilling a ~ 150 – $190 \mu\text{m}$ hole into the center of the indentation. Pressure was determined by measuring the fluorescence of a ruby sphere.³⁶ In most cases a pressure medium was not used to avoid any potential sample contamination, but for some of the IR scans the sample was diluted with dry potassium bromide. All samples were sealed to a starting pressure of ~ 0.1 GPa within the inert argon atmosphere before removing from the glovebox.

IID. Raman Spectroscopy. Samples were excited with a 532 nm diode laser, focused through a 20 \times long working distance objective (NA = 0.40) and Raman light was collected in the backscatter geometry through a 50 μm confocal pinhole and two narrow-band notch filters (Ondax). The Raman signal was collected using a Princeton Instrument spectrograph SP2750 (Trenton, NJ) and dispersed off an 1800 or 300 groove/mm grating on to a liquid nitrogen cooled CCD, providing a maximum spectral resolution of $< 2 \text{ cm}^{-1}$. The spectrometer was calibrated with the emission lines from neon assuring a wavelength accuracy of $< 1 \text{ cm}^{-1}$. Laser-induced damage was avoided by keeping the beam power at $\sim 1 \text{ mW}$ with exposure times less than 300 s. As a result of these measurement conditions, no change was observed in the

reaction pressure, suggesting that photoinduced chemistry was not important in this energy/laser power range. The Raman spectrum of $\text{Li}_3\text{C}_6\text{N}_9$ was acquired on a Renishaw inVia Raman microscope with 785 nm excitation due to high fluorescence at shorter excitation wavelengths.

IIE. IR Spectroscopy. A Varian 670-IR spectrometer was used to collect mid-IR absorption from ~ 600 to 4000 cm^{-1} . IR light was generated by a Globar source and collected by a liquid nitrogen-cooled HgCdTe detector after passing through the sample with a pair of reflecting objectives. Reference spectra were obtained using the same DAC after the cell was decompressed and the diamonds were cleaned.

IIF. X-ray Diffraction. Powder X-ray diffraction (PXRD) was collected at the High Pressure Collaborative Access Team (HPCAT), beamline 16-IDB, of the Advanced Photon Source (APS), Argonne National Laboratory. A monochromatic beam with a wavelength of 0.4066 Å was focused to a spot size of $\sim 5 \times 7 \mu\text{m}^2$. Diffraction data were recorded using a MAR image plate and the images were processed using the fit2d(v12.077) data analysis program.³⁷ Lattice parameters were obtained through full profile refinement using the Le Bail method, as implemented in GSAS with EXPGUI.^{38,39} Rietveld refinement was attempted but judged unacceptable due to inadequacies in powder averaging statistics.

IIG. Sample Annealing. In one run, the high-pressure sample was annealed to increase the extent of reaction before measuring Raman spectra and visible absorption. The DAC with the $\text{LiN}(\text{CN})_2$ at 20 GPa was placed in an oven at 373 K for 14 h. It was then allowed to cool to room temperature before Raman and visible absorption data were collected.

III. RESULTS

IIIA. Diffraction. The crystal structure of lithium dicyanamide was previously reported as monoclinic with space group $P2_1/c$ (no.13).²¹ We confirm this result and obtained ambient-pressure lattice parameters of $a = 5.3169(13) \text{ Å}$, $b = 5.2964(13) \text{ Å}$, $c = 11.6454(11) \text{ Å}$, and $\beta = 101.245(12)^\circ$, which closely match the previously reported results.²¹ We note that the calculated lattice parameters obtained after DFT relaxation ($a = 5.308 \text{ Å}$, $b = 5.249 \text{ Å}$, $c = 11.498 \text{ Å}$, $\beta = 101.55^\circ$) are in good agreement with this result. Within this structure, there are chains of lithium atoms that occupy alternating tetrahedral and octahedral sites and propagate down the c -axis (Figure 1). The dicyanamide molecules act as bridging units in the a – b plane between Li polyhedra, of which nitrogen atoms form the vertices.

As pressure is increased from 0.1 to 3.6 GPa, a expands slightly from its starting value, b and c decrease monotonically, while β increases. We note that the error bars are relatively large due to pressure-induced peak broadening, but the observed increase in a might be related with an anisotropic compression mechanism (discussed below). As the pressure is further increased to 9.5 GPa, b and c continue to decrease, and β 's rate of increase slows. Between 3 and 9.5 GPa, a decreases almost linearly, and after 9.5 GPa the XRD patterns could no longer be reliably described using the starting $P2_1/c$ structure, indicating a transition to another crystalline phase.

At 13.5 GPa we observed a peak at 9.28° that continued to shift to higher angles as pressure was applied up to 22.2 GPa, and some crystalline features were observed to the highest pressure measured. As shown in Figure 2, these features indicate that, whereas most crystalline diffraction is undetect-

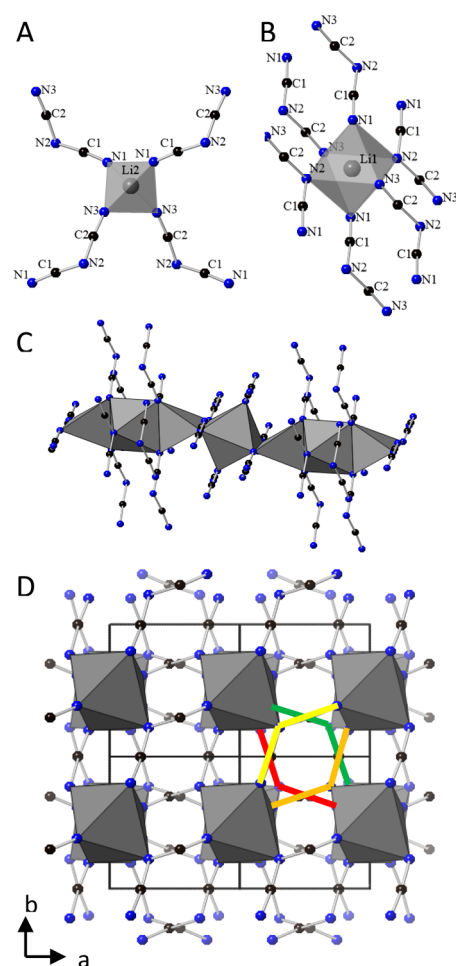


Figure 1. Structure of $\text{LiN}(\text{CN})_2$. (A) Tetrahedral coordination of lithium by four dicyanamide groups. (B) Octahedral coordination of lithium by six dicyanamide groups. (C) View perpendicular to the c -axis consisting of alternating chains of edge-sharing tetrahedra and octahedral lithium atoms that are parallel to the c -axis. (D) View of four unit cells along the c -axis where each dicyanamide ion bridges three different chains of Li polyhedra. The colored lines highlight the bonding of individual dicyanamide groups.

able above ca. 15 GPa, the sample is not completely amorphous.

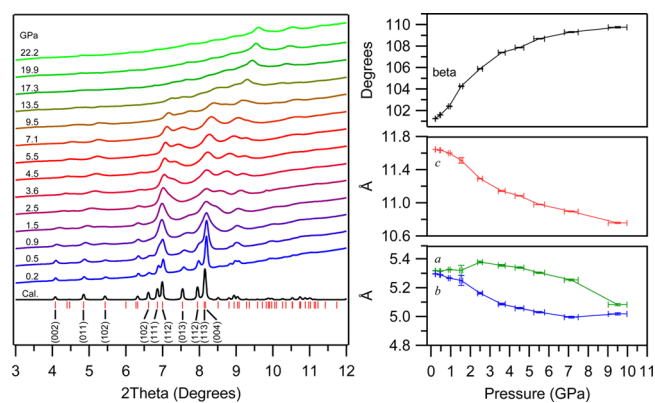


Figure 2. (Left) PXRD of $\text{LiN}(\text{CN})_2$ as a function of pressure. (Right) Lattice parameters with pressure.

IIIB. Raman Spectroscopy. The isolated dicyanamide ion has C_{2v} symmetry and possesses nine fundamental vibrational modes. According to group-theory analysis, solid lithium dicyanamide has 72 vibrational modes. The irreducible representation of all zone-center modes is given as $M = 16A_g + 19A_u + 17B_g + 20B_u$, of which 33 (A_g, B_g) are Raman active and 39 (A_u, B_u) are IR active. Table 1 shows assignments for

Table 1. Experimental Raman and IR Modes for $\text{LiN}(\text{CN})_2$ at 0.1 GPa^a

vibrational mode	obsd in (intensity)	mode character	exptl observations (cm^{-1})	theory (cm^{-1})
First Order				
ν_1	R (s)	$\nu_s(\text{N}\equiv\text{C})$	2243	2235 ^b
ν_2	IR (m)	$\nu_s(\text{N}-\text{C})$	944	943–946 ^b
ν_2	R (w)	$\nu_s(\text{N}-\text{C})$	943	939–941 ^b
ν_3	R (w)	δ_s bend	671	650–653 ^b
ν_4	R (s)	γ_s bend	227	230
ν_{4a}	R (w)	γ_s bend	206	206
ν_{4b}	R (w)	γ_s bend	240	244
ν_5	R (w)	γ_s bend	549	530–532 ^b
ν_6	R (w)	γ_{as} bend	554	554–561 ^b
ν_7	R (s)	$\nu_{as}(\text{N}\equiv\text{C})$	2166	2180–2181 ^b
ν_8	IR (s)	$\nu_{as}(\text{N}-\text{C})$	1346	1423 ^b
ν_9	R	γ_{as} bend		468–530 ^b
	R (m)	lattice	145	145
	R (w)	lattice	138	137
	R (w)	lattice	121	117–128 ^b
	R (m)	lattice	106	103
	R (m)	lattice	91	88–99 ^b
	R (m)	lattice	78	74–77 ^b

^aDFPT calculations for this study were conducted at 1 atm. ^bDFPT gives a large number of discrete modes with this character due to crystal field splitting. For simplicity, the range of these modes has been compared with experimental data in the context of the fundamentals of the isolated ion.

observed Raman and IR modes of $\text{LiN}(\text{CN})_2$ compared with results from DFPT calculations. Given the large number of vibrational modes possible in the crystalline state and the lower number of modes observed, we report mode numbers following fundamental assignments in the context of the isolated dicyanamide with the realization that some of these modes will be split in the solid by crystal-field effects. The peaks in the Raman and IR were fit using Lorentzian peak shapes.

The highest-frequency Raman mode observed at 2234 cm^{-1} is assigned to the $\text{C}\equiv\text{N}$ symmetric stretch (ν_1). This assignment is in agreement with our calculations (2235 cm^{-1}) and comparable with the symmetric stretch of Na dicyanamide of 2225 cm^{-1} reported by Perkins.⁴⁰ The shift observed between Li and Na dicyanamides can be explained by differences in cations and through crystal structure effects. Our assignment is in contrast with Reckeweg et al., who reported the symmetric $\text{C}\equiv\text{N}$ stretch at 2305 cm^{-1} ; the mode observed by Reckeweg et al. at 2236 cm^{-1} was assigned to a combination of $\text{C}-\text{N}$ symmetric and asymmetric stretching modes.²¹ The assignment by Reckeweg et al. is likely related to a typographical error as the combination band at 2236 cm^{-1} was reported to have strong intensity, whereas the ν_1 fundamental was reported as having very weak intensity. Because the fundamental symmetric mode should have very strong Raman intensity, this discrepancy can be resolved by

simply switching the reported assignments in their table entry (which are consecutive). The $\text{C}\equiv\text{N}$ asymmetric stretching mode (ν_7) was observed at 2166 cm^{-1} and is in reasonable agreement with our calculated value of 2180 cm^{-1} . Reckeweg et al.²¹ reported the $\text{C}\equiv\text{N}$ asymmetric stretching mode at 2168 cm^{-1} , which is in agreement with this work, whereas this mode was observed at 2174 cm^{-1} for the Na analogue (Perkins).⁴⁰ For the isolated C_{2v} molecule, the symmetric (A_1) and asymmetric (B_2) $\text{C}\equiv\text{N}$ stretching modes are active in both the Raman and IR. In the solid state, these modes are split into A_g , A_u , B_g , and B_u components, but the Raman and IR frequencies remain nearly coincident. We were unable to observe these stretching modes in the IR due to the strong absorption of the diamond anvils used in our experiments (between ca. $2000\text{--}2400\text{ cm}^{-1}$).

The $\text{C}\text{--}\text{N}$ symmetric stretching mode (ν_2) was observed in the IR and the Raman at 944 and 943 cm^{-1} , respectively, and is in general agreement with our calculations and the previous study by Reckeweg et al.²¹ For the Na salt, the $\text{C}\text{--}\text{N}$ symmetric stretch was observed at 937 cm^{-1} (Raman) and 931 cm^{-1} (IR).⁴⁰ The $\text{C}\text{--}\text{N}$ asymmetric stretch (ν_8) was observed in the IR at 1346 cm^{-1} , but not observed in the Raman where it could possibly be obscured by the strong T_{2g} diamond phonon near 1333 cm^{-1} . The calculated frequency of the $\text{C}\text{--}\text{N}$ asymmetric stretching mode at 1422 cm^{-1} is significantly shifted from the observed position and the origin of this discrepancy is presently unclear. However, the observation of this mode at 1339 cm^{-1} in the IR by Reckeweg et al. is in good agreement with the present study (no Raman frequency was reported previously).²¹

The symmetric bending (ν_3) mode was observed in the Raman at 671 cm^{-1} and is shifted from our calculated value of 650 cm^{-1} . Reckeweg et al. reported this mode at 682 cm^{-1} , whereas Perkins observed this mode at 671 cm^{-1} for the Na salt.^{21,40} We tentatively assign the ν_4 symmetric bending mode at 227 cm^{-1} on the basis of comparison of Raman intensity with our calculations. However, two additional bands are observed at 206 and 240 cm^{-1} , and calculations reveal that they both have character similar to that of ν_4 (symmetric bending).

The asymmetric bending modes (ν_5 , ν_6 , and ν_9) are difficult to discern on the basis of similarities in character and frequency. Perkins was unable to make definitive assignments for the Na salt, but from a detailed analysis of the combination modes he was able to reach the tentative assignment of ν_5 (A_2) at 544 cm^{-1} , ν_6 (B_1) at 526 cm^{-1} , and ν_9 (B_2) at 517 cm^{-1} .⁴⁰ On the basis of our DFPT calculations, we suggest assignments of ν_5 at 549 cm^{-1} and ν_6 554 cm^{-1} and ν_9 is unobserved experimentally but occurs at 530 cm^{-1} in the calculations.

We report seven low-frequency lattice mode vibrations, which are observed with Raman for the first time. The lattice modes are sensitive to any increase in pressure and quickly broaden. The last seven peaks are lattice vibrations located at 145 , 138 , 121 , 106 , 91 , and 78 cm^{-1} . All seven modes agree well with our calculated values (145 , 140 , 117 , 104 , 89 , 77 cm^{-1}).

IIIC. Raman Spectroscopy under Pressure. With this understanding of the vibrational spectroscopy of the starting material, we now turn our attention to the behavior during compression. As pressure is increased, the frequencies of the carbon nitrogen triple bond stretching modes (ν_1 , ν_7) increase until 6.6 GPa . At 7.6 GPa the ν_1 mode splits into two components separated by 5 cm^{-1} . Figure 3 shows these two peaks continuing to increase in frequency with increasing pressure as they slowly diverge from each other. The

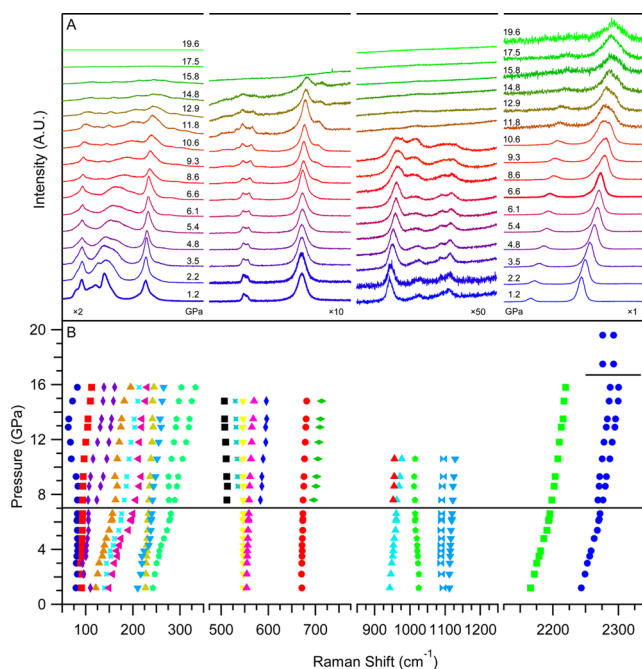


Figure 3. (A) Raman spectra of $\text{LiN}(\text{CN})_2$ with pressure at room temperature. Spectra have been normalized to the most intense peak in each panel for clarity. Each spectral range has been scaled by the value at the bottom of each panel. (B) Pressure dependence of the observed Raman modes of $\text{LiN}(\text{CN})_2$.

asymmetric mode becomes too weak to be accurately fitted beyond 18 GPa .

The frequency of the symmetric bending mode (ν_3) at 671 cm^{-1} increases linearly with increasing pressure, but a new shoulder appears on the high-frequency side at 7.6 GPa . Both of these peaks are visible until 14.8 GPa . The peak at 554 cm^{-1} that has been tentatively assigned as ν_6 has almost no change in frequency versus pressure. At 7.6 GPa a peak forms on the high-frequency side and is separated by $+24\text{ cm}^{-1}$. The mode at 549 cm^{-1} , tentatively assigned as ν_5 , has little change in position with increasing pressure. At 8.6 GPa a shoulder appears on the low-frequency side of ν_5 and is separated by -11 cm^{-1} . At 7.6 GPa , however, a new peak does form on the low-frequency side of ν_5 , at -35 cm^{-1} . These five peaks have little change in frequency versus pressure and beyond 14.8 GPa no Raman peaks were observed between 400 and 750 cm^{-1} .

The frequency of the ν_4 mode at 227 cm^{-1} gradually increases with increasing pressure up to 16 GPa , which is similar to the peak at 240 cm^{-1} . At 7.6 GPa the peak at 240 cm^{-1} gradually splits into two and both peaks continue to higher frequency with increasing pressure. The peak at 206 cm^{-1} also shifts with increasing pressure and crosses the ν_4 position near 4.3 GPa . After 5 GPa the rate of frequency increase with pressure decreases. The lattice modes 145 , 138 , and 121 cm^{-1} follow the same trends of increasing frequency with increasing pressure.

IIID. IR Spectroscopy under Pressure. The IR frequency of the ν_2 near mode 944 cm^{-1} increases with increasing pressure until 9.3 GPa ; however, there is a notable change in the slope of the pressure dependence near 4.4 GPa (Figure 2). Above $\sim 9\text{ GPa}$ the frequency of this mode appears to decrease with additional pressure increase. A new peak appears at 5.7 GPa on the high-frequency side of ν_2 that is shifted by $+47$

cm^{-1} and shows positive frequency correlation with increasing pressure.

The asymmetric N–C stretching mode near 1348 cm^{-1} (ν_8), which was only observed in the IR, has a linear frequency increase with increasing pressure until 6.9 GPa, at which point a new peak emerges on the low-frequency side (Figure 4). The

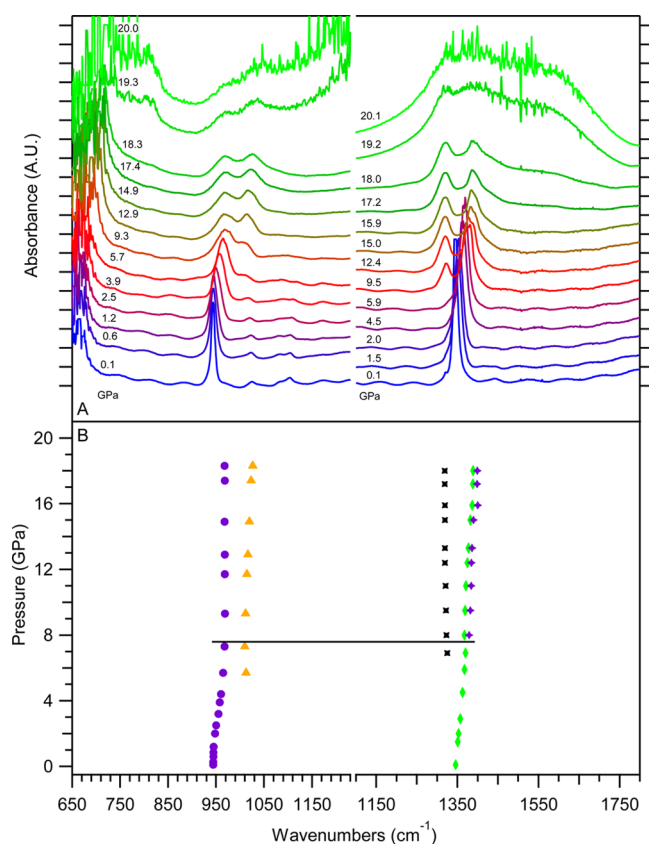


Figure 4. (A) IR spectra of $\text{LiN}(\text{CN})_2$ with pressure at room temperature. Unaltered IR spectra have been offset for clarity. The spectra on the right were obtained with potassium bromide dilution due to strong absorbance. One tick mark on the vertical axis equals one absorbance unit (A.U.) (B) Pressure dependence of the observed IR modes of $\text{LiN}(\text{CN})_2$.

new peak has a slight frequency decrease with increasing pressure. The original ν_8 peak continues to increase in frequency until 8 GPa, where it splits into two components separated by $\sim 13 \text{ cm}^{-1}$.

III. High-Pressure Annealing. Pristine $\text{LiN}(\text{CN})_2$ at ambient conditions is translucent and colorless, owing to its ionic and molecular nature. As the pressure was increased from 0 to 15 GPa, the material's color remained unchanged when inspected under visible light illumination. When the pressure was increased past 15 GPa, the material began to transition from colorless to a translucent red color, which became darker as the pressure was increased to 20 GPa. This absorption behavior is similar to that of a previously reported C_3N_4 carbon nitride material, which is indicative of similar structural motifs in both compounds.⁴¹ To accelerate this transition and ensure more complete reaction, the sample was annealed at 373 K and 20 GPa for 14 h. After annealing, the material exhibited a brilliant red color, with a visible absorption edge near 540 nm ($2.3 \pm 0.1 \text{ eV}$) (Figure 5).⁴²

The Raman spectrum of the sample above ~ 15 GPa has only one remaining feature from the starting molecule (the symmetric $\text{C}\equiv\text{N}$ stretch, ν_1), and four new broad bands appear with features similar to those of amorphous carbons.⁴³ These new features become significantly stronger after annealing, but no new modes that might arise from subsequent crystallization were observed. After annealing, ν_1 completely disappears, which indicates that heating provides thermal energy to accelerate the extent of polymerization, or possibly activates an additional reaction mechanism. For the annealed sample, the so-called “D” and “G”-like bands can be observed between 1400 and 1600 cm^{-1} , but the D peak is partially obscured by the Raman scattering from the diamond anvils. The G band is located at 1598 cm^{-1} , and the D band is located at 1392 cm^{-1} . Two-ring vibrational modes are observed at 745 and 1021 cm^{-1} , which are shifted to higher frequency than previous observations due to the high-pressure conditions. Koglin et al. identified similar peaks in melamine, which might be a suitable analog for polymerized $\text{LiN}(\text{CN})_2$.^{44,45}

IV. DISCUSSION

At low pressure our results agree with previous reports on $\text{LiN}(\text{CN})_2$ and other dicyanamides using Raman/IR spectroscopies and PXRD. The unit cell dimensions were similar to the

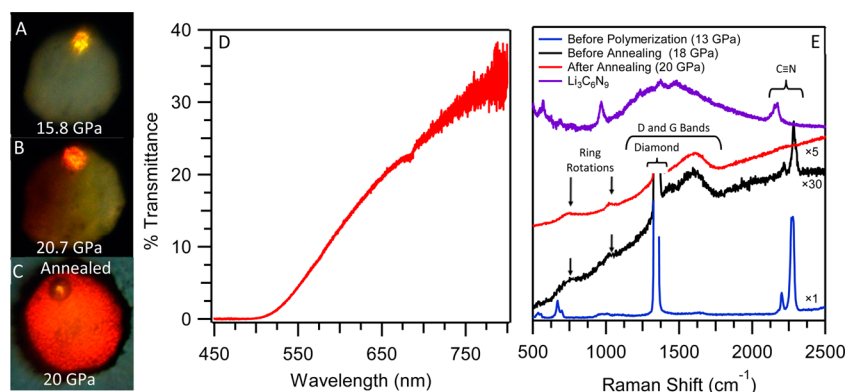


Figure 5. (A) Optical transmitted image of $\text{LiN}(\text{CN})_2$ in a DAC at 15.8 GPa before polymerization. A ruby sphere is used to measure the pressure and is located at the top of each image. (B) $\text{LiN}(\text{CN})_2$ just after polymerization. (C) $\text{LiN}(\text{CN})_2$ after annealing at 373 K for 14 h. (D) The visible transmittance of annealed $\text{LiN}(\text{CN})_2$. (E) Raman of lithium dicyanimide at 13 GPa before polymerization, at 18 GPa before annealing and 20 GPa after annealing. For comparison, the Raman spectrum of lithium tricyanomelaminide on a glass substrate at 1 atm has also been plotted.

previously reported values, and the IR and Raman data at the starting pressures show quantitative agreement with previous studies.^{17,21,40} As the material is compressed to 7.6 GPa, most of the peaks in the Raman and IR have a monotonic trend of increasing frequency with increasing pressure. This agrees with our diffraction data that show the unit cell volume is decreasing, and thus the bond lengths get shorter, which causes them to shift to higher frequencies. Both lattice parameters *b* and *c* decrease monotonically over the entire pressure interval. However, between 0 and 3 GPa, *a* appears to increase slightly with pressure. This effect might be related to negative linear compressibility and has been observed in many other systems including some cyanide-based compounds.^{46–48} The monoclinic structure necessitates that the *a*-direction is not a principal compression axis; however, analysis of the compressibility tensor using the PASCAL Software⁴⁹ does indeed show linear expansion along the lattice vector [+0.9526, 0, -0.3043]. By examination of the crystal structure, it seems reasonable that LiN(CN)₂ could exhibit mild linear negative compressibility over a limited pressure range. Baughman et al. reported several similarities that materials with linear negative compressibility share, one of them being “hinge-like” structures.⁵⁰ The dicyanamide molecules do indeed form “hinges” where each nitrogen is associated with a different chain of alternating tetrahedral and octahedral lithium ions, thereby allowing for stretch densification. This behavior could explain the observed increase in *a* and should be investigated in more detail in future studies.

On the basis of spectroscopic and PXRD observations, a polymorphic phase transition occurs around 9 GPa. The first signs of this transition begin at ~7.5 GPa where we observe seven new peaks in the Raman and two new peaks in the IR, as well as slope changes in the pressure dependence of their frequencies. It is important to note that the original peaks associated with the molecular crystal are still present and did not change remarkably in frequency and intensity. This indicates that the overall nature of bonding remains largely unchanged after the transition; i.e., the crystal remains molecular and is a new polymorph of LiN(CN)₂. These new peaks arrive just before the PXRD patterns change near 9 GPa, and the diffraction data can no longer be fitted using the starting *P2/c* structural model. All of these observations are consistent with a first-order phase transition in crystalline LiN(CN)₂, likely due to a lower-symmetry form based on the increased number of vibrational modes observed.

Above ~18 GPa, the spectroscopic data point toward a more dramatic chemical (polymeric) transformation involving the formation of new covalent bonds. All of the molecular Raman peaks except ν_1 were no longer detectable above ~16 GPa. There are also drastic changes in the IR near 1550 cm⁻¹, with the onset of broad absorption bands above 17 GPa. Above 19 GPa, IR transmission associated with these broad bands decreased drastically until the signal was saturated beyond the detectable limit, and all IR features of the starting material are lost beyond 19–20 GPa. These changes in the Raman and IR spectra suggest a pressure-induced reaction between cyanide units and concomitant bond order changes from *sp* to *sp*².

It has been established that certain cyanide-based molecules can undergo pressure-induced polymerization.^{13,51–58} For dicyanamides specifically, it has been reported that when heated at ambient pressure they will undergo a trimerization reaction to form tricyanomelamine (C₆N₉³⁻) compounds. A possible mechanism for the pressure-induced reaction observed

here is a scheme similar to the previously reported, thermally induced trimerization reaction at atmospheric pressure.^{25–27}

This trimerization reaction would involve three dicyanamides, each contributing a nitrile group, resulting in the formation of triazine rings and comparable to the tricyanomelamine product. The broad IR feature observed here above 17 GPa (Figure 4) is likely composed of two peaks at 1450 and 1550 cm⁻¹. Li₃C₆N₉ exhibits similar features showing strong absorbance across the same spectral region,²⁷ and the position of these bands are generally consistent with the formation of triazine rings.^{59,60} The Raman spectra above 15 GPa also share three prominent features with Li₃C₆N₉: C≡N stretching, ring rotation modes, and a broad band central band in the region of *sp*² C=N/C=C stretching. We note that the central band observed for Li₃C₆N₉ (Figure 5e) is more pronounced near 1400 cm⁻¹ due to contributions from the glass substrate.

Above 18 GPa most of the X-ray diffraction signal is very broad and essentially undetectable, indicating a significant loss of long-range correlations and tendency toward amorphization. Nevertheless, PXRD patterns still exhibit some crystalline features beyond 20 GPa, indicating that the material is not completely amorphous after the initial polymerization event.

Although the pressure-induced material shows spectroscopic similarities with thermally trimerized LiN(CN)₂, this material changes again after high-pressure thermal annealing at 373 K. After heating, all evidence for C≡N stretching vanishes, indicating an increased extent of polymerization and possibly a new, thermally activated reaction mechanism. As with the material obtained before annealing, the presence of the D/G peaks and the peaks at 743 and 1024 cm⁻¹ are evidence of ring formation in the final product.^{44,61} The Raman data show that these modes become more intense after annealing, which is potentially associated with the rings being in strained conformations immediately after reaction, which are unable to relax until the annealing process occurs.

Unlike other cyanide-based materials that have been observed to turn opaque after pressure-induced polymerization, the final LiN(CN)₂ product remains transparent. It is likely that other systems graphitize to a much larger extent, but in the case of LiN(CN)₂, the remaining Li atoms present in the structure prevent polymerization over longer length scales and, thus, an optical gap remains in the polymerized material exhibiting an absorption edge near 540 nm. This absorption edge is slightly more transparent than the C₃N₄ carbon nitride material prepared by Purdy et al.⁴¹ For the trimerized structure presented by Jurgens et al. the C₆N₉³⁻ anions are approximately planar and are surrounded by six sodium ions.²⁵ The sodium ions are isolating the C₆N₉³⁻ anions from each other, preventing reaction into a more extended network. If Na₃C₆N₉ is heated further, it will decompose instead of polymerizing.²⁵ It is likely that this situation is analogous to the lithium dicyanamide case presented here where Li ions prevent longer-range polymerization in a similar fashion, although the extent of polymerization is greater than in pure Li₃C₆N₉ based on the absence of detectable nitrile groups in the Raman spectrum.

Further characterization on the resulting material was not possible because the material is not air stable and reacts violently when exposed to ambient air, which prevents further characterization after recovery. Possible explanations for the air sensitivity include lithium reacting with oxygen or moisture in air, as well as the formation of unstable rings with carbon–carbon or nitrogen–nitrogen bonds. It is our speculation that

through disruption, the lithium ions are preventing more organized and/or larger extended networks from forming. In future studies, it would be of interest to recover the material under inert conditions to further examine the extent of polymerization.

V. CONCLUSION

Using a DAC, we studied $\text{LiN}(\text{CN})_2$ with Raman and IR spectroscopy and synchrotron X-ray diffraction data to understand how its chemical nature changes with increasing pressure and to determine a new pathway for polymerization of CN networks. We have characterized the structure and vibrational properties at low pressure with results in correspondence with previous reports. Upon compression, our results suggest that $\text{LiN}(\text{CN})_2$ exhibits negative linear compressibility up to ~ 3 GPa. At ~ 8 GPa we observe a polymorphic phase transition by the emergence new peaks in the Raman and IR, as well as structural changes via PXRD. Above 15 GPa the material begins to react, and spectroscopic signatures of aromatic carbon–nitrogen bonds are observed, with strong similarities to the thermal trimerization product of $\text{LiN}(\text{CN})_2$ at atmospheric pressure. The final product is recoverable to atmospheric pressure but is highly reactive and not stable in air.

■ AUTHOR INFORMATION

Corresponding Authors

*D. W. Keefer. E-mail: keefer.derek@gmail.com. Telephone: 814-863-0556.

*T. A. Strobel. E-mail: tstrobel@ciw.edu. Telephone: 202-478-8943.

Notes

The authors declare no competing financial interest.

■ ACKNOWLEDGMENTS

We thank J. Smith and R. Hrubik for assistance with XRD measurements. This work was supported by DARPA under ARO Contract No. 31P4Q-3-I-0005. Portions of this work were performed at HPCAT (Sector 16), Advanced Photon Source (APS), Argonne National Laboratory. HPCAT operations are supported by DOE-NNSA under Award No. DE-NA0001974 and DOE-BES under Award No. DE-FG02-99ER45775, with partial instrumentation funding by NSF. APS is supported by DOE-BES, under Contract No. DE-AC02-06CH11357. D.Y.K. acknowledges the Texas Advanced Computing Center (TACC) at the University of Texas at Austin and Argonne Leadership Computing Facility (ALCF) which is a DOE Office of Science User Facility supported under Contract No. DEAC02-06CH11357 for providing high-performance computing resources and the support of NSAF Grant No. U1530402.

■ REFERENCES

- (1) Teo, K. B. K.; Ferrari, A. C.; Fanchini, G.; Rodil, S. E.; Yuan, J.; Tsai, J. T. H.; Laurenti, E.; Tagliaferro, A.; Robertson, J.; Milne, W. I. Highest Optical Gap Tetrahedral Amorphous Carbon. *Diamond Relat. Mater.* **2002**, *11*, 1086–1090.
- (2) Liu, A. Y.; Cohen, M. L. Prediction of New Low Compressibility Solids. *Science* **1989**, *245*, 841–842.
- (3) Teter, D. M.; Hemley, R. J. Low-Compressibility Carbon Nitrides. *Science* **1996**, *271*, 53–55.
- (4) Wang, X.; Bao, K.; Tian, F.; Meng, X.; Chen, C.; Dong, B.; Li, D.; Liu, B.; Cui, T. Cubic Gauche-CN: A Superhard Metallic Compound

Predicted via First-Principles Calculations. *J. Chem. Phys.* **2010**, *133*, 044512.

- (5) Dong, H.; Oganov, A. R.; Zhu, Q.; Qian, G.-R. The Phase Diagram and Hardness of Carbon Nitrides. *Sci. Rep.* **2015**, *5*, 9870.

- (6) Brito, W. H.; da Silva-Araujo, J.; Chacham, H. g-C₃N₄ and Others: Predicting New Nanoporous Carbon Nitride Planar Structures with Distinct Electronic Properties. *J. Phys. Chem. C* **2015**, *119*, 19743–19751.

- (7) Sandre, E.; Pickard, C. J.; Colliex, C. What are the Possible Structures for CN_x Compounds? The Example of C₃N. *Chem. Phys. Lett.* **2000**, *325*, 53–60.

- (8) Hart, J. N.; Claeysens, F.; Allan, N. L.; May, P. W. Carbon Nitride: Ab Initio Investigation of Carbon-Rich Phases. *Phys. Rev. B: Condens. Matter Mater. Phys.* **2009**, *80*, 174111.

- (9) Chen, K.; Chai, Z.; Li, C.; Shi, L.; Liu, M.; Xie, Q.; Zhang, Y.; Xu, D.; Manivannan, A.; Liu, Z. Catalyst-Free Growth of Three-Dimensional Graphene Flakes and Graphene/g-C₃N₄ Composite for Hydrocarbon Oxidation. *ACS Nano* **2016**, *10*, 3665–3673.

- (10) Zhang, Z.; Zhang, J.; Chen, N.; Qu, L. Graphene Quantum Dots: An Emerging Material for Energy-Related Applications and Beyond. *Energy Environ. Sci.* **2012**, *5*, 8869–8890.

- (11) Cao, X. H.; Yin, Z. Y.; Zhang, H. Three-Dimensional Graphene Materials: Preparation, Structures and Application in Supercapacitors. *Energy Environ. Sci.* **2014**, *7*, 1850–1865.

- (12) Lin, Z. Y.; Waller, G. H.; Liu, Y.; Liu, M. L.; Wong, C. P. Simple Preparation of Nanoporous Few-Layer Nitrogen-Doped Graphene for Use as an Efficient Electrocatalyst for Oxygen Reduction and Oxygen Evolution Reactions. *Carbon* **2013**, *53*, 130–136.

- (13) Gou, H.; Yonke, B. L.; Epshteyn, A.; Kim, D. Y.; Smith, J. S.; Strobel, T. A. Pressure-Induced Polymerization of P(CN)₃. *J. Chem. Phys.* **2015**, *142*, 194503.

- (14) Fitzgibbons, T. C.; Guthrie, M.; Xu, E.-s.; Crespi, V. H.; Davidowski, S. K.; Cody, G. D.; Alem, N.; Badding, J. V. Benzene-Derived Carbon Nanofibers. *Nat. Mater.* **2014**, *14*, 43–47.

- (15) Sakashita, M.; Yamawaki, H.; Aoki, K. FT-IR Study of the Solid State Polymerization of Acetylene under Pressure. *J. Phys. Chem.* **1996**, *100*, 9943–9947.

- (16) Aoki, K.; Usuba, S.; Yoshida, M.; Kakudate, Y.; Tanaka, K.; Fujiwara, S. Raman Study of the Solid-State Polymerization of Acetylene at High Pressure. *J. Chem. Phys.* **1988**, *89*, 529.

- (17) Irran, E.; Jürgens, B.; Schnick, W. Trimerization of Alkali Dicyanides M[N(CN)₂] and Formation of Tricyanomelaminates M₃[C₆N₉] (M = K, Rb) in the Melt: Crystal Structure Determination of Three Polymorphs of K[N(CN)₂], Two of Rb[N(CN)₂], and One of K₃[C₆N₉] and Rb₃[C₆N₉] from X-ray Powder Diffraction. *Chem. - Eur. J.* **2001**, *7*, 5372–5381.

- (18) Jürgens, B.; Irran, E.; Schnick, W. Synthesis and Characterization of the Rare-Earth Dicyanides Ln[N(CN)₂]₃ with Ln = La, Ce, Pr, Nd, Sm, and Eu. *J. Solid State Chem.* **2005**, *178*, 72–78.

- (19) Starynowicz, P. Structure of Cesium Dicyanide. *Acta Crystallogr., Sect. C: Cryst. Struct. Commun.* **1991**, *47*, 2198–2199.

- (20) Irran, E.; Jürgens, B.; Schnick, W. Synthesis, Crystal Structure Determination from X-ray Powder Diffraction and Vibrational Spectroscopy of the Tricyanomelamine Monohydrates M₃[C₆N₉]·H₂O (M = K, Rb). *Solid State Sci.* **2002**, *4*, 1305–1311.

- (21) Reckeweg, O.; DiSalvo, F. J.; Schulz, A.; Blaschkowski, B.; Jagiella, S.; Schleid, T. Synthesis, Crystal Structure, and Vibrational Spectra of the Anhydrous Lithium Dicyanide Li[N(CN)₂]. *Z. Anorg. Allg. Chem.* **2014**, *640*, 851–855.

- (22) Jürgens, B.; Hoppe, H. A.; Schnick, W. Synthesis, Crystal Structure, Vibrational Spectroscopy, and Thermal Behaviour of Lead Dicyanide Pb[N(CN)₂]₂. *Solid State Sci.* **2002**, *4*, 821–825.

- (23) Kurmoo, M.; Kepert, C. J. Hard Magnets Based on Transition Metal Complexes with the Dicyanide Anion, [N(CN)₂]⁻. *New J. Chem.* **1998**, *22*, 1515–1524.

- (24) Lotsch, B. V.; Schnick, W. Towards Novel C-N Materials: Crystal Structures of Two Polymorphs of Guanidinium Dicyanide and their Thermal Conversion into Melamine. *New J. Chem.* **2004**, *28*, 1129–1136.

- (25) Jurgens, B.; Irran, E.; Schneider, J.; Schnick, W. Trimerization of NaC_2N_3 to $\text{Na}_3\text{C}_6\text{N}_9$ in the Solid: Ab Initio Crystal Structure Determination of Two Polymorphs of NaC_2N_3 and of $\text{Na}_3\text{C}_6\text{N}_9$ from X-ray Powder Diffractometry. *Inorg. Chem.* **2000**, *39*, 665–670.
- (26) Cairns, T. L.; Larchar, A. W.; McKusick, B. C. The Trimerization of Nitriles at High Pressures. *J. Am. Chem. Soc.* **1952**, *74*, 5633–5636.
- (27) Purdy, A. P.; Houser, E.; George, C. F. Lithium Dicyanamide, its Reactions with Cyanuric Chloride, and the Crystal Structures of $\text{LiN}(\text{CN})_2(\text{MeCN})_2$ and $\text{LiCN}(\text{C}_5\text{H}_5\text{N})_2$. *Polyhedron* **1997**, *16*, 3671–3679.
- (28) Lotsch, B. V.; Schnick, W. Thermal Conversion of Guanlyurea Dicyanamide into Graphitic Carbon Nitride via Prototype CN_x Precursors. *Chem. Mater.* **2005**, *17*, 3976–3982.
- (29) Jurgens, B.; Irran, E.; Senker, J.; Kroll, P.; Muller, H.; Schnick, W. Melem (2,5,8-triamino-tri-s-triazine), an Important Intermediate During Condensation of Melamine Rings to Graphitic Carbon Nitride: Synthesis, Structure Determination by X-ray Powder Diffractometry, Solid-State NMR, and Theoretical Studies. *J. Am. Chem. Soc.* **2003**, *125*, 10288–10300.
- (30) Collins, C.; Thadhani, N.; Iqbal, Z. Shock-Compression of C-N Precursors for Possible Synthesis of Beta- C_3N_4 . *Carbon* **2001**, *39*, 1175–1181.
- (31) Aoki, K.; Kakudate, Y.; Yoshida, M.; Usuba, S.; Fujiwara, S. Solid-State Polymerization of Cyanoacetylene into Conjugated Linear-Chains Under Pressure. *J. Chem. Phys.* **1989**, *91*, 778–782.
- (32) Dymont, V. P.; Nekrashevich, E. M.; Starchenko, I. M. Synthesis of a Bulk Crystalline Phase of Carbon Nitride. *JETP Lett.* **1998**, *68*, 498–501.
- (33) Baroni, S.; de Gironcoli, S.; Dal Corso, A.; Giannozzi, P. Phonons and Related Crystal Properties from Density-Functional Perturbation Theory. *Rev. Mod. Phys.* **2001**, *73*, 515–562.
- (34) Giannozzi, P. QUANTUM ESPRESSO: A Modular and Open-Source Software Project for Quantum Simulations of Materials. *J. Phys.: Condens. Matter* **2009**, *21*, 395502.
- (35) Perdew, J. P.; Burke, K.; Ernzerhof, M. Generalized Gradient Approximation Made Simple. *Phys. Rev. Lett.* **1996**, *77*, 3865–3868.
- (36) Mao, H. K.; Xu, J.; Bell, P. M. Calibration of the Ruby Pressure Gauge to 800-kbar Under Quasi-Hydrostatic Conditions. *J. Geophys. Res.* **1986**, *91*, 4673–4676.
- (37) Hammersley, A. P.; Svensson, S. O.; Hanfland, M.; Fitch, A. N.; Hausermann, D. Two-Dimensional Detector Software: From Real Detector to Idealised Image or Two-Theta Scan. *High Pressure Res.* **1996**, *14*, 235–248.
- (38) Larson, A. C.; Von Dreele, R. B. General Structure Analysis System (GSAS), Los Alamos National Laboratory Report LAUR 86-748, 2004.
- (39) Desgreniers, S. High-density phases of ZnO: Structural and compressive parameters. *Phys. Rev. B: Condens. Matter Mater. Phys.* **1998**, *58*, 14102–14105.
- (40) Perkins, A. Raman and Infrared Spectra of the Dicyanamide Ion. In *Developments in Applied Spectroscopy*; Ferraro, J. R., Ziomek, J. S., Eds.; Springer: New York, 1963; Vol. 2, pp 43–51.
- (41) Purdy, A. P.; Callahan, J. H. Syntheses of Sublimable Carbon Nitride Materials. *Main Group Chem.* **1998**, *2*, 207–213.
- (42) Tauc, J. Optical Properties and Electronic Structure of Amorphous Ge and Si. *Mater. Res. Bull.* **1968**, *3*, 37–46.
- (43) Ferrari, A. C.; Robertson, J. Interpretation of Raman Spectra of Disordered and Amorphous Carbon. *Phys. Rev. B: Condens. Matter Mater. Phys.* **2000**, *61*, 14095–14107.
- (44) Koglin, E.; Kip, B. J.; Meier, R. J. Adsorption and Displacement of Melamine at the Ag/Electrolyte Interface Probed by Surface-Enhanced Raman Microprobe Spectroscopy. *J. Phys. Chem.* **1996**, *100*, 5078–5089.
- (45) Andreyev, A.; Akaishi, M.; Golberg, D. Synthesis of Nanocrystalline Nitrogen-Rich Carbon Nitride Powders at High Pressure. *Diamond Relat. Mater.* **2002**, *11*, 1885–1889.
- (46) Cairns, A. B.; Catafesta, J.; Levelut, C.; Rouquette, J.; van der Lee, A.; Peters, L.; Thompson, A. L.; Dmitriev, V.; Haines, J.; Goodwin, A. L. Giant Negative Linear Compressibility in Zinc Dicyanoaurate. *Nat. Mater.* **2013**, *12*, 212–216.
- (47) Li, W.; Probert, M. R.; Kosa, M.; Bennett, T. D.; Thirumurugan, A.; Burwood, R. P.; Parinello, M.; Howard, J. A. K.; Cheetham, A. K. Negative Linear Compressibility of a Metal–Organic Framework. *J. Am. Chem. Soc.* **2012**, *134*, 11940–11943.
- (48) Goodwin, A. L.; Keen, D. A.; Tucker, M. G. Large Negative Linear Compressibility of $\text{Ag}_3[\text{Co}(\text{CN})_6]$. *Proc. Natl. Acad. Sci. U. S. A.* **2008**, *105*, 18708–18713.
- (49) Cliffe, M. J.; Goodwin, A. L. PASCAL: A Principal Axis Strain Calculator for Thermal Expansion and Compressibility Determination. *J. Appl. Crystallogr.* **2012**, *45*, 1321–1329.
- (50) Baughman, R. H.; Stafström, S.; Cui, C.; Dantas, S. O. Materials with Negative Compressibilities in One or More Dimensions. *Science* **1998**, *279*, 1522–1524.
- (51) Aoki, K.; Baer, B. J.; Cynn, H. C.; Nicol, M. High-Pressure Raman Study of One-Dimensional Crystals of the very Polar Molecule Hydrogen Cyanide. *Phys. Rev. B: Condens. Matter Mater. Phys.* **1990**, *42*, 4298–4303.
- (52) Chapman, K. W.; Halder, G. J.; Chupas, P. J. Pressure-Induced Amorphization and Porosity Modification in a Metal–Organic Framework. *J. Am. Chem. Soc.* **2009**, *131*, 17546–17547.
- (53) Li, K.; Zheng, H.; Ivanov, I. N.; Guthrie, M.; Xiao, Y.; Yang, W.; Tulk, C. A.; Zhao, Y.; Mao, H.-k. $\text{K}_3\text{Fe}(\text{CN})_6$: Pressure-Induced Polymerization and Enhanced Conductivity. *J. Phys. Chem. C* **2013**, *117*, 24174–24180.
- (54) Nesting, D. C.; Badding, J. V. High-Pressure Synthesis of sp^2 -Bonded Carbon Nitrides. *Chem. Mater.* **1996**, *8*, 1535–1539.
- (55) Yoo, C. S.; Nicol, M. Kinetics of a Pressure-Induced Polymerization Reaction of Cyanogen. *J. Phys. Chem.* **1986**, *90*, 6732–6736.
- (56) Tomasino, D.; Chen, J.-Y.; Kim, M.; Yoo, C.-S. Pressure-Induced Phase Transition and Polymerization of Tetracyanoethylene (TCNE). *J. Chem. Phys.* **2013**, *138*, 094506–094506–10.
- (57) Khazaei, M.; Arai, M.; Sasaki, T.; Kawazoe, Y. Polymerization of Tetracyanoethylene under Pressure. *J. Phys. Chem. C* **2013**, *117*, 712–720.
- (58) Yamawaki, H.; Aoki, K.; Kakudate, Y.; Yoshida, M.; Usuba, S.; Fujiwara, S. Infrared Study of Phase Transition and Chemical Reaction in Tetracyanoethylene under High Pressure. *Chem. Phys. Lett.* **1992**, *198*, 183–187.
- (59) Lotsch, B. V.; Schnick, W. From Triazines to Heptazines: Novel Nonmetal Tricyanomelaminates as Precursors for Graphitic Carbon Nitride Materials. *Chem. Mater.* **2006**, *18*, 1891–1900.
- (60) Li, X.; Zhang, J.; Shen, L.; Ma, Y.; Lei, W.; Cui, Q.; Zou, G. Preparation and Characterization of Graphitic Carbon Nitride through Pyrolysis of Melamine. *Appl. Phys. A: Mater. Sci. Process.* **2009**, *94*, 387–392.
- (61) Rodil, S. E.; Ferrari, A. C.; Robertson, J.; Milne, W. I. Raman and Infrared Modes of Hydrogenated Amorphous Carbon Nitride. *J. Appl. Phys.* **2001**, *89*, 5425.